

# Effects of Growth Orientations and Epitaxial Strains on Phase Stability of $\text{HfO}_2$ Thin Films

Shi Liu\* and Brendan M Hanrahan\*

*Sensors & Electron Devices Directorate, U.S. Army Research Laboratory, Adelphi, Maryland 20783, United States.*

E-mail: upennliushi@gmail.com; brendan.m.hanrahan.civ@mail.mil

## Abstract

The discovery of ferroelectricity in both pure and doped  $\text{HfO}_2$ -based thin films have revitalized the interest in using ferroelectrics for nanoscale device applications. To take advantage of this silicon-compatible ferroelectric, fundamental questions such as the origin of ferroelectricity and better approach to controlled realization of ferroelectricity at the nanoscale need to be addressed. The emergence of robust polarization in  $\text{HfO}_2$ -based thin films is considered as the cumulative effect of various extrinsic factors such as finite size effects and surface/interface effects of small grains, compressive stress, dopants, oxygen vacancies, and electric fields. The kinetic effects of phase transitions and their potential impacts on the emergence of ferroelectricity in  $\text{HfO}_2$  are not well understood. In this work, we construct the transition paths between different polymorphs of hafnia with density functional theory calculations and variable-cell nudged elastic band technique. We find that the transition barriers depend strongly on the mechanical boundary conditions and the transition from the tetragonal phase to the polar orthorhombic phase is a fast process kinetically. The effects of growth orientations and epitaxial strains on the relative stability of different phases of  $\text{HfO}_2$  are investigated. The two orthorhombic phases, polar  $Pca2_1$  and non-polar  $Pbca$ , become

thermodynamically stable in (111)-oriented thin films over a wide range of epitaxial strain conditions. This work suggests a potential avenue to better stabilize the ferroelectric phase in  $\text{HfO}_2$  thin films through substrate orientation engineering.

# Introductions

Ferroelectrics characterized by the switchable spontaneous polarization have long been considered as a candidate material to realize low-power high-speed nonvolatile memories and logic devices.<sup>1-3</sup> However, the difficulty of integrating perovskite ferroelectrics into complementary metal-oxide-semiconductor (CMOS) processes<sup>4</sup> has hindered device scaling to the sub-100 nm regime.<sup>5</sup> The discovery of ferroelectricity in both pure and doped HfO<sub>2</sub> thin films<sup>6-11</sup> have revitalized the interest in using ferroelectrics for nanoscale device applications<sup>12</sup> because HfO<sub>2</sub> is a well-studied CMOS-compatible gate dielectric that is thermodynamically stable on silicon.<sup>13</sup> Moreover, contrary to conventional perovskite-based ferroelectric thin films where the depolarization field often leads to the instability of out-of-plane polarization,<sup>14-16</sup> HfO<sub>2</sub>-based thin films possess robust electrical polarization at the nanoscale, ideal for device miniaturization.<sup>6</sup> It is suggested that HfO<sub>2</sub> may well be a new type of ferroelectric materials that only exhibits spontaneous polarization at the nanometer length scale but not in the bulk form.<sup>17</sup>

The observation of ferroelectricity in HfO<sub>2</sub> is unexpected, given that this simple binary oxide has been studied extensively for decades as high- $\kappa$  dielectrics.<sup>18</sup> Bulk HfO<sub>2</sub> adopts the monoclinic (M)  $P2_1/c$  phase at the room temperature and pressure, and transforms to the tetragonal (T)  $P4_2/nmc$  phase and the cubic  $Fm\bar{3}m$  phase with increasing temperature, and becomes the orthorhombic (OA)  $Pbca$  phase at higher pressure. All these phases are centrosymmetric and thus non-polar. Börscke *et al.* first reported the presence of ferroelectricity in thin films of SiO<sub>2</sub>-doped hafnium oxide with a thickness of 10 nm.<sup>6</sup> Since then, many divalent and trivalent dopants were found to be able to induce ferroelectricity in hafnia thin films.<sup>7-9,19</sup> Robust polarization of  $10\mu\text{C}/\text{cm}^2$  was observed even in dopant-free hafnia thin films in a thickness range of 4-20 nm.<sup>20</sup>

The origin of ferroelectricity in HfO<sub>2</sub>-based thin films has attracted intensive studies in recent years. Combined experimental and theoretical studies eventually lead to the conclusion that the polar orthorhombic (PO)  $Pca2_1$  phase is most likely responsible for the

ferroelectricity.<sup>10,21–24</sup> Based on density functional theory (DFT) calculations, the M phase is the most stable phase, followed by the polar PO phase and the non-polar T phase.<sup>21,22,24</sup> The stabilization of the metastable PO phase in thin films is attributed to a variety of extrinsic factors such as finite size effects and surface/interface effects associated with small grain size,<sup>10,20,24–27</sup> strains of different origins,<sup>28,29</sup> dopants,<sup>9,19,30–32</sup> oxygen vacancies,<sup>11,33</sup> and electric fields.<sup>29</sup>

In the phenomenological surface energy model developed by Materlik *et al.* that takes into account the surface energy contribution to the phase stability, the hafnia gains of nanometer size ( $< 4$  nm) will favor the ferroelectric phase because of the lower surface energy of the PO phase relative to that of the M phase.<sup>24</sup> Batra *et al.* evaluated the surface energies of different phases of hafnia with DFT and found that the PO phase has lower (001) surface energy but higher (100) and (010) surface energies than those of the M phase.<sup>25</sup> They also found that the surface energies of the T phase are consistently lower than the M phase for all surface planes, suggesting a possible initial formation of the non-polar T phase at the nanoscale due to the surface effects followed by a transition to the ferroelectric PO phase.<sup>25</sup>

The epitaxial compressive strain is considered to play an important role in inducing the ferroelectric PO phase.<sup>22,29</sup> However, DFT calculations have shown that neither hydrostatic pressure nor biaxial compressive stress alone is enough to make the polar phase the most stable phase. Therefore, the application of external electric fields is required to drive the non-polar to polar phase transition,<sup>29</sup> which may explain the “wake-up effect” in hafnia films.<sup>9,34,35</sup> The presence of oxygen vacancies is often detrimental to the device functionality by causing leakage current, aging, and fatigue in ferroelectrics, but is proposed to be beneficial for realizing the ferroelectric PO phase.<sup>27</sup> Recent experiments demonstrated an enhanced ferroelectricity in sub-10 nm dopant-free hafnia thin films by lowering the oxidant dose (thus increasing the oxygen vacancy concentration) during growth,<sup>27</sup> consistent with first-principles results that ionized oxygen vacancies may stabilize the metastable PO phases.<sup>36</sup> It appears that the emergence of ferroelectricity in  $\text{HfO}_2$  thin films is indeed the cumulative

effect of various extrinsic factors.

Previous studies on epitaxial strain engineering of ferroelectricity have mostly focused on thin films grown on (00*l*)-oriented substrates.<sup>37</sup> There is now growing interest in applying biaxial strain along other crystallographic planes such as (101) and (111) by growing thin films on substrates of different cuts.<sup>38</sup> The substrate orientation offers an unconventional route to tune the mechanical boundary conditions that can substantially affect the phase stability and ferroelectric domain morphologies. For example, DFT calculations suggest that (111)-oriented BaTiO<sub>3</sub> thin films have drastically different strain-driven phase transitions from the (001)-oriented thin films, and (110)-oriented BaTiO<sub>3</sub> may support three distinct monoclinic phases that are not present in bulk BaTiO<sub>3</sub>.<sup>39</sup> Experimental work on (111)-oriented PbZr<sub>*x*</sub>Ti<sub>1-*x*</sub>O<sub>3</sub> thin films revealed a high-density, nanotwinned domain morphology consisting of degenerate polarization variants that enable both direct 180° and multi-step 90° switching.<sup>40,41</sup> In this regard, it is important to explore the effect of substrate orientation on the ferroelectric properties of HfO<sub>2</sub>.<sup>42</sup> Recently, it was discovered that Hf<sub>0.5</sub>Zr<sub>0.5</sub>O<sub>2</sub> thin films grown on (001)-oriented La<sub>0.7</sub>Sr<sub>0.3</sub>MnO<sub>3</sub>/SrTiO<sub>3</sub> substrates predominantly adopt the (111) orientation and display large polarization values up to 34 μC/cm<sup>2</sup>,<sup>17</sup> further highlighting the potential impact of crystal orientations on functional properties. Moreover, ferroelectric HfO<sub>2</sub>-based films are often polycrystalline consisting of grains of different orientations such that only grains with the polar axis along the surface normal direction will contribute to the out-of-plane polarization in (001)-oriented films. Growing unconventionally oriented films such as (111)-oriented films will guarantee stable out-of-plane polarization, which is beneficial for the usage of polycrystalline films for high density integration which can be realized by downscaling the lateral dimensions.<sup>43</sup>

In this work, we start by examining the ideal transition barriers between different phases of HfO<sub>2</sub> with first-principles methods, aiming to reveal the underlying multi-well potential energy surface that is critical for the understanding of the kinetic effects of phase transitions. We find that the three low-energy phases, *P*2<sub>1</sub>/*c*, *Pca*2<sub>1</sub>, and *Pbca*, are separated by signifi-

cant barriers ( $> 0.1$  eV/f.u.), and the high-temperature tetragonal  $P4_2/nmc$  phase serves as an important intermediate structure bridging different phases. Moreover, the transformation from the tetragonal phase to the polar phase is kinetically fast, and tuning the mechanical boundary conditions can make it the most favorable transition path. Growing unconventionally oriented crystals on substrates of different cuts provides an additional knob to control the mechanical boundary conditions. We evaluate the energies of different polymorphs of hafnia with biaxial deformations applied in the  $\{100\}$ ,  $\{110\}$ , and  $\{111\}$  planes. Our calculations reveal that the two orthorhombic phases, polar  $Pca2_1$  and non-polar  $Pbca$ , become more stable than the monoclinic phase in (111)-oriented films over a range of epitaxial strain conditions, suggesting a new route to better stabilize the polar phase in  $\text{HfO}_2$  thin films through substrate orientation engineering.

## Computational Methods

### *ab initio* studies on the phase transition paths

We use the variable-cell nudged elastic band (VC-NEB) technique<sup>44</sup> implemented in the USPEX code<sup>45-47</sup> to study the transition paths between different polymorphs of hafnium oxides. Specifically, we investigate following solid-solid phase transitions:  $T \rightarrow PO$ ,  $T \rightarrow OA$ ,  $T \rightarrow M$ , and  $OA \rightarrow PO$ . Each transition path is constructed by 40 images. The *ab initio* calculations are carried out using local density approximation implemented in Quantum Espresso<sup>48</sup> with ultrasoft pseudopotentials from the Garrity, Bennett, Rabe, Vanderbilt high-throughput pseudopotential set.<sup>49</sup> A plane-wave cutoff of 50 Ry, a charge density cutoff of 250 Ry, and a reciprocal-space resolution of  $0.26 \text{ (\AA}^{-1})$  for  $k$ -points generation are used. We choose  $0.025 \text{ eV/\AA}$  for the root-mean-square (RMS) forces on images as the halting criteria condition for VC-NEB calculations. The variable elastic constant scheme<sup>50</sup> is utilized by setting the spring constant between the neighboring images in the range of  $2.0 - 6.0 \text{ eV/\AA}^2$ .

The performance of NEB calculations requires a predefined atomic mapping scheme upon

which the initial transition path consisting of a discrete set of configurations can be constructed, typically by a linear interpolation of the Cartesian coordinates between the initial and final states. VC-NEB introduces additional lattice degrees of freedom.<sup>44</sup> Therefore, there could be multiple transition paths connecting two phases depending on the choice of atomic and crystal axis (orientation) mapping. To distinguish different crystal orientation mapping schemes, we use following conventions for the initial state: (1) Unit cells of four HfO<sub>2</sub> formula units (12 atoms) of different phases are reoriented to have their  $a$  and  $c$  axes corresponding to the smallest and the largest lattice constants, respectively. (2) The  $a$ ,  $b$ , and  $c$  axes are aligned along the Cartesian axes  $X$ ,  $Y$ , and  $Z$ , respectively. The unit cell of OA phase has 24 atoms and the lattice constant along the  $X$  axis is  $2a$ . As an example, for the PO  $\rightarrow$  T phase transition, one natural choice of crystal orientation mapping is  $a \rightarrow a'$ ,  $b \rightarrow a'$ , and  $c \rightarrow c'$ , denoted as  $X_{a'}^a Y_{a'}^b Z_{c'}^c$  where the superscripts represent the initial state and the subscripts represent the final state. Another two orientation mapping schemes are  $X_{c'}^a Y_{a'}^b Z_{a'}^c$  and  $X_{a'}^a Y_{c'}^b Z_{a'}^c$ . Though one might expect the natural choice  $X_{a'}^a Y_{a'}^b Z_{c'}^c$  would give rise to a lower transition barrier, we later found it was not the case, indicating the importance of exploring all orientation mapping schemes. For a given orientation mapping, we decide the atomic mapping between the initial and final states by pairing atoms (of the same type) that are closest in distance. This simple protocol in most cases result in a unique atomic mapping scheme. In Figure 1b, we report only the minimum energy path connecting two phases.

***ab initio* studies on the effects of crystal growth orientations**

We explore three biaxial strain states corresponding to the epitaxial growth of (100)-, (110)-, and (111)-oriented films. The following four phases are considered: M, T, PO, and OA. For a cubic structure, the measurement axes distinguishing different growth orientations are illustrated in Figure 1a: the (001)-oriented film has [100] along  $X$ , [010] along  $Y$ , [001] along  $Z$ ; similarly, the (011)-oriented film has [100] along  $X$ , [01 $\bar{1}$ ] along  $Y$ , and [011] along  $Z$ ; the [111]-oriented system has [ $1\bar{1}0$ ] along  $X$ , [ $11\bar{2}$ ] along  $Y$ , and [111] along  $Z$ . The  $XY$

plane is chosen as the epitaxial plane and the  $Z$  axis is considered as the surface normal direction of a thin film.

Because the four phases of  $\text{HfO}_2$  have symmetry lower than the cubic phase, there are three different  $\{001\}$  planes for the M, PO, and OA phases and two for the T phase, three  $\{101\}$  planes and three  $\{111\}$  planes for all four phases, respectively. Considering a unit cell with lattice constants  $a \neq b \neq c$ , we introduce following notations to represent different orientations: the three  $\{001\}$  planes are labeled as  $X[a00]Y[0b0]Z[00c]$ ,  $X[0a0]Y[0c0]Z[00b]$ , and  $X[0b0]Y[0c0]Z[00a]$ ; the three  $\{101\}$  planes are  $X[a00]Y[0b\bar{c}]Z[0bc]$ ,  $X[0b0]Y[a0\bar{c}]Z[a0c]$ , and  $X[00c]Y[a\bar{b}0]Z[ab0]$ ; the three  $\{111\}$  planes are  $X[a\bar{b}0]Y[ab\bar{2}c]Z[abc]$ ,  $X[a0\bar{c}]Y[a\bar{2}bc]Z[abc]$ , and  $X[0b\bar{c}]Y[\bar{2}abc]Z[abc]$ . Here again we assume the short axis  $a$  of the unit cell is along  $[100]$  and the long axis  $c$  is along  $[001]$ . The notation is easy to understand. For example,  $X[00c]Y[a\bar{b}0]Z[ab0]$  means the  $[00c]$  crystal axis is along the  $X$  axis,  $[a\bar{b}0]$  is along the  $Y$  axis, and  $[ab0]$  is along the  $Z$  axis (see illustrations in Figure 1b), which will represent the ideal  $(110)$  plane when  $a = b = c$ . It is noted that because the unit cell of OA phase has 24 atoms and the lattice constant along the  $[100]$  direction is  $2a$ , its  $[022]$  and  $[122]$  directions coincide with the  $[011]$  and  $[111]$  directions of the 12-atom unit cell. In following discussions we will ignore this subtle difference and will only use notations based on the 12-atom unit cell.

For each phase, we first construct a supercell with the prescribed crystal orientation and then fully relax the lattice vectors and atomic positions. After the equilibrium lattice parameters are obtained, the biaxial strain is applied in  $XY$  plane by scaling the lattice vectors along  $X$  and  $Y$  while conserving the in-plane lattice angle  $\gamma$ . We make a special note here that the biaxial strain states studied in this way do not consider the effect of in-plane shear strains as the value of  $\gamma$  is fixed. The internal coordinates are fully optimized while allowing the  $Z$  axis to relax, resembling the response of epitaxially strained thin films.

# Results and Discussions

**Phase Transitions of HfO<sub>2</sub> polymorphs** Figure 2a reports the optimized lattice parameters of different polymorphs using LDA and Figure 2b shows the minimum energy paths obtained with VC-NEB. The forward and reverse transition barriers are reported in Table 1. The enthalpy of the T phase is considered as the zero point, and the enthalpies of M, OA, and PO phases are  $-128$ ,  $-95$ , and  $-75$  meV/f.u., respectively, consistent with previous DFT results.<sup>21,22,24</sup> We find that the three phases, M, OA, and PO, are separated by large barriers ( $> 100$  meV/f.u.  $\approx 1160$  K). Consequently, M, OA, and PA phases are less likely to go through direct transitions between them. In contrary, the transition from the T phase to the other three phases only need to overcome a small enthalpy barrier,  $\Delta H^\ddagger(\text{T} \rightarrow \text{OA}) = 67$ ,  $\Delta H^\ddagger(\text{T} \rightarrow \text{OA}) = 32$ ,  $\Delta H^\ddagger(\text{T} \rightarrow \text{M}) = 13$  meV/f.u., respectively. Therefore, we propose that the T phase is likely to serve as the “precursor” phase during the phase transitions between M, OA, and PO. We also find that the transformation from the T phase to the ferroelectric PO phase is faster *kinetically* than to the non-polar orthorhombic OA phase despite the OA phase being lower in enthalpy. This suggests that even in the absence of electric fields, the formation of ferroelectric PO phase is feasible because of the relatively low kinetic barrier.

We closely examine and compare the two phase transitions that have the low barriers:  $\text{T} \rightarrow \text{M}$  and  $\text{T} \rightarrow \text{PO}$ . It is evident from Figure 3 that the transition  $\text{T} \rightarrow \text{M}$  involves a large change in lattice constants and angles: the long axis of the T phase increases by 2% and the angle  $\beta$  (between  $a$  and  $c$  axes) increases by 11%, a clear sign of large shear deformation. In comparison, the transition  $\text{T} \rightarrow \text{PO}$  undergoes a modest volume variation through the exchange of short and long axes,  $X^a Y^a Z^c \rightarrow X_c Y_b Z_{a'}$ . This process can be understood as a “90° rotation” about the  $b$  axis along which the polarization is developed in the PO phase. The volume first decreases before reaching the transition state (that has the highest enthalpy) and then increases after overcoming the barrier.

The substantial shear deformation in the  $\text{T} \rightarrow \text{M}$  phase transition hints at a stronger response of the transition barrier to the mechanical boundary conditions. To test this hy-

pothesis, we carry out conventional NEB calculations where the lattice constants are fixed to the values of the T phase, assuming the T phase is the “precursor” phase during the growth of thin films.<sup>51</sup> As revealed in Figure 3c, constraining the lattice degrees of freedom drastically affects the transition paths. First, the “artificial” M phase with the same lattice constants of the T phase, denoted as  $M_T$ , becomes a high energy phase. We find that the  $M_T$  phase experiences highly anisotropic stresses,  $\sigma_{13} = \sigma_{31} = -10.8$  GPa and  $\frac{1}{3}\text{tr}(\sigma_{ij}) = 1.37$  GPa. It is also in line with previous studies that a compressive pressure tends to destabilize the M phase. The energy of the non-polar OA phase remains lower than that of ferroelectric PO phase. Second, the transition  $T \rightarrow M$  now involves the ferroelectric PO phase as the intermediate structure, in agreement with the dopant-induced phase transition route observed experimentally.<sup>30,31</sup> Moreover, the PO phase is the local minimum along the  $T \rightarrow M$  transition path and its transformation to the M phase needs to overcome a large barrier. Finally, we find that the transition  $T \rightarrow OA$  is kinetically slower than the transition  $T \rightarrow PO$ , and OA and PO phases are separated by a large barrier, making the direct transition between them difficult. Therefore, under the constraint of lattice degrees of freedom, the transition  $T \rightarrow OA$  is kinetically favored over all the other possible phase transitions. These results highlight the kinetic and strain effects on the emergence of ferroelectric phase in  $\text{HfO}_2$  thin films. Specifically, when the shear strain required for the  $T \rightarrow M$  transition is inaccessible, the T phase is more likely to become the ferroelectric PO phase *kinetically* even though the non-polar OA phase is still favored *thermodynamically*. In this regard, growing  $\text{HfO}_2$ -based films on unconventionally oriented substrates may introduce appropriate mechanical boundary conditions that enhance the ferroelectricity, thus inspiring our following investigations.

**Effects of Crystal Orientations** We first study the conventional (001)-oriented films. The effect of epitaxial strain in (001) plane ( $X[a00]Y[0b0]Z[00c]$ ) on the relative stability of different phases of hafnia was already explored previously in ref. 29 with DFT using PBE exchange-correlation functional.<sup>52,53</sup> Here we systematically investigate the effects of biaxial

deformations in all  $\{001\}$  planes on the energetics of M, T, OA, and PO phases with LDA. The results are illustrated in Figure 4 which shows the energy as a function of the planar area in the  $XY$  plane. We first compare the relative phase stability due to the misfit strains in the (100), (010), and (001) planes separately (Figure 4 top). The trend in phase stability due to equibiaxial deformations in the (001) plane revealed by our LDA calculations agrees with the PBE results reported in ref. 29: the compressive strain tends to stabilize the two orthorhombic phases OA and PO over the M phase, while the energy of the non-polar OA phase is always lower than the polar PO phase. Similar trend is also found for equibiaxial deformations enforced in the (100) plane. However, the M phase remains the lowest-energy phase in (010)-oriented films.

For the convenience of distinguishing different orientations, we introduced the convention that the  $a$ ,  $b$ , and  $c$  axes of the unit cell are aligned along the  $[100]$ ,  $[010]$ , and  $[001]$  directions, respectively (Figure 1b). However, it is possible that the  $c$  axis of the crystal will align along the  $[100]$  or  $[010]$  direction of the substrate during the growth, leading to (100)- or (010)-oriented thin films grown on (001)-oriented substrates. For this reason, it is important to compare energies of all different orientations using the planar area as a measurement of in-plane stress (Figure 4 bottom). This comparison takes into account the possibility that  $\text{HfO}_2$  may adopt an orientation different from the underlying substrate. We find that the compressive stress induces a  $M \rightarrow \text{OA}$  transition when the planar area is around  $25 \text{ \AA}^2$ , whereas the ferroelectric PO phase never becomes the lowest energy phase.

We further quantify the effects of biaxial deformations in all  $\{101\}$  planes on the stability of M, OA, and PO phases with results reported in Figure 5. It is found that OA and PO phases become thermodynamically favored over the M phase in (101)-oriented films when the unit cell during the growth has the  $[a0c]$  lattice vector aligned along the surface normal (Figure 5 top). When such constraint is lifted, the M phase is favored over a wide range of epitaxial strain conditions (Figure 5 bottom).

The results for (111)-oriented films reveal some interesting features (Figure 6a). Similar to

the (001)-oriented films, the epitaxial compressive stress drives the M  $\rightarrow$  OA phase transition. The critical misfit strain  $\epsilon$  is  $\approx -2.6\%$  (in reference to the equilibrium M phase,  $\epsilon = 1.0 - \sqrt{S/S_M^0}$ ) at which the M and OA phases are close in energy. Interestingly, both OA and PO phases are more stable than the M phase over a wide range of compressive strains beyond the critical strain. Notably, the OA phase becomes the local energy minimum when the epitaxial misfit strain is  $\approx -4.1\%$ , suggesting the possibility to realize the orthorhombic phase *thermodynamically* by growing (111)-oriented thin films on selective substrates that offer the right misfit strains.

The ferroelectric PO phase consistently has energy higher than the non-polar OA phase, but the energy difference is small ( $< 40$  meV/f.u.). Two mechanisms may lead to the formation of ferroelectric phase in thin films. Thermodynamically, the presence of an external field along the polar axis will favor the PO phase and induce the OA  $\rightarrow$  PO transition. This is confirmed by estimating the free energy  $G$  under an electric field along the surface normal direction ( $\mathcal{E}_{111}$ ),  $G = E_{\text{DFT}} - \mathcal{E}_{111}P_{[111]}V_{\text{f.u.}}$ , where  $E_{\text{DFT}}$  is the DFT energy per formula unit and  $P_{[111]}$  is the polarization along the [111] direction (inset of Figure 6b). The effect of [111] electric fields on the free energy difference between PO and OA phases ( $\Delta G_{\text{PO-OA}}$ ) is illustrated in Figure 6b, which clearly shows the stabilization of the PO phase over the OA phase for electric fields of magnitude higher than 4 MV/cm. Kinetically, as revealed by NEB calculations, the transition from the T phase to the PO phase is faster than to the OA phase. Therefore, if the T phase forms first during the high temperature annealing in thin film preparation process, a significant portion of the T phase may transform to the PO phase because of the low activation energy of the T  $\rightarrow$  PO transition.

## Conclusions

In summary, we have investigated the kinetic effects of phase transitions on the emergence of ferroelectricity in HfO<sub>2</sub> thin films by quantifying the transition barriers between different

polymorphs of hafnia with density functional theory calculations. The multi-well potential energy surface obtained with the variable-cell nudged elastic band technique suggests that the mixture of different phases often presented in HfO<sub>2</sub>-based thin films has both kinetic and thermodynamic reasons. We propose the tetragonal  $P4_2/nmc$  phase, likely formed during the annealing process at high temperatures, is the key “precursor” phase, responsible for the formation of monoclinic and orthorhombic phases because of the low transition barriers. One important finding is that the transition from the tetragonal phase to the polar orthorhombic  $Pca2_1$  phase is kinetically faster than the transition to the competing non-polar orthorhombic  $Pbca$  phase though the latter is favored thermodynamically. Additionally, the transition barriers depend strongly on the mechanical boundary conditions. In particular, when the shear deformation required for the tetragonal to monoclinic phase transition becomes inaccessible (e.g., clamping by grains or capping electrodes), the formation of the monoclinic phase will be suppressed whereas the formation of the polar orthorhombic phase is favored.

Growing differently-oriented crystals on substates of unconventional cuts offers a new modality to tune the mechanical boundary conditions. We systematically investigate the effects of growth orientations and epitaxial strains on the relative stability of different phases of HfO<sub>2</sub>. In agreement with previous studies, the biaxial compressive stress will drive the monoclinic to orthorhombic transition. Notably, the two orthorhombic phases become more stable than the monoclinic phase in (111)-oriented thin films over a wide range of epitaxial strain conditions. It is feasible to make the  $Pbca$  phase the equilibrium phase by growing (111)-oriented films on substates providing the right misfit strains. The energy of the polar  $Pca2_1$  phase is found to be consistently higher than the non-polar  $Pbca$  phase. The presence of electric fields along the surface normal direction will drive the system to the polar phase thermodynamically. Another possible mechanism leading to the formation of ferroelectric  $Pca2_1$  phase would be the transformation of the high-temperature tetragonal phase thanks to the low phase transition barrier. These results provide useful insights into the origin of ferroelectricity in HfO<sub>2</sub>-based thin films and important implications for better control of the

ferroelectric phase through substrate orientation engineering.

## Acknowledgments

SL is supported by SEDD Distinguished Postdoc Fellowship at US Army Research Laboratory.

## References

- (1) Buck, D. A. Ferroelectrics for Digital Information Storage and Switching. M.Sc. thesis, MIT Digital Computer Laboratory, 1952.
- (2) Ross, I. M. Semiconductive Translating Device. 1957; U.S. Patent 2791760A.
- (3) Scott, J. F. Applications of Modern Ferroelectrics. *Science* **2007**, *315*, 954–959.
- (4) Pinnow, C.-U.; Mikolajick, T. Material Aspects in Emerging Nonvolatile Memories. *J. Electrochem. Soc.* **2004**, *151*, K13.
- (5) McAdams, H. et al. A 64-Mb Embedded FRAM Utilizing a 130-nm 5LM Cu/FSG Logic Process. *IEEE Journal of Solid-State Circuits* **2004**, *39*, 667–677.
- (6) Böscke, T. S.; Müller, J.; Bräuhaus, D.; Schröder, U.; Böttger, U. Ferroelectricity in Hafnium Oxide Thin Films. *Appl. Phys. Lett.* **2011**, *99*, 102903.
- (7) Müller, J.; Schröder, U.; Böscke, T. S.; Müller, I.; Böttger, U.; Wilde, L.; Sundqvist, J.; Lemberger, M.; Kücher, P.; Mikolajick, T.; Frey, L. Ferroelectricity in Yttrium-Doped Hafnium Oxide. *J. Appl. Phys.* **2011**, *110*, 114113.
- (8) Mueller, S.; Mueller, J.; Singh, A.; Riedel, S.; Sundqvist, J.; Schroeder, U.; Mikolajick, T. Incipient Ferroelectricity in Al-Doped HfO<sub>2</sub> Thin Films. *Adv. Funct. Mater.* **2012**, *22*, 2412–2417.

- (9) Schroeder, U.; Yurchuk, E.; Müller, J.; Martin, D.; Schenk, T.; Polakowski, P.; Adelman, C.; Popovici, M. I.; Kalinin, S. V.; Mikolajick, T. Impact of Different Dopants on the Switching Properties of Ferroelectric Hafnium Oxide. *Jpn. J. Appl. Phys.* **2014**, *53*, 08LE02.
- (10) Park, M. H.; Lee, Y. H.; Kim, H. J.; Kim, Y. J.; Moon, T.; Kim, K. D.; Müller, J.; Kersch, A.; Schroeder, U.; Mikolajick, T.; Hwang, C. S. Ferroelectricity and Antiferroelectricity of Doped Thin HfO<sub>2</sub>-Based Films. *Adv. Mater.* **2015**, *27*, 1811–1831.
- (11) Pal, A.; Narasimhan, V. K.; Weeks, S.; Littau, K.; Pramanik, D.; Chiang, T. Enhancing Ferroelectricity in Dopant-Free Hafnium Oxide. *Appl. Phys. Lett.* **2017**, *110*, 022903.
- (12) Pešić, M.; Künneth, C.; Hoffmann, M.; Mulaosmanovic, H.; Müller, S.; Breyer, E. T.; Schroeder, U.; Kersch, A.; Mikolajick, T.; Slesazeck, S. A Computational Study of Hafnia-Based Ferroelectric Memories: from Ab Initio via Physical Modeling to Circuit Models of Ferroelectric Device. *J. Comput. Electron.* **2017**, *16*, 1236–1256.
- (13) Gutowski, M.; Jaffe, J. E.; Liu, C.-L.; Stoker, M.; Hegde, R. I.; Rai, R. S.; Tobin, P. J. Thermodynamic Stability of High- $\kappa$  Dielectric Metal Oxides ZrO<sub>2</sub> and HfO<sub>2</sub> in Contact with Si and SiO<sub>2</sub>. *MRS Proceedings* **2002**, *716*, B3.2.
- (14) Batra, I. P.; Wurfel, P.; Silverman, B. D. Phase Transition, Stability, and Depolarization Field in Ferroelectric Thin Films. *Phys. Rev. B* **1973**, *8*, 3257–3265.
- (15) Wurfel, P.; Batra, I. P. Depolarization-Field-Induced Instability in Thin Ferroelectric Films—Experiment and Theory. *Phys. Rev. B* **1973**, *8*, 5126–5133.
- (16) Ma, T.; Han, J.-P. Why Is Nonvolatile Ferroelectric Memory Field-Effect Transistor Still Elusive? *IEEE Electron Device Letters* **2002**, *23*, 386–388.
- (17) Wei, Y.; Nukala, P.; Salverda, M.; Matzen, S.; Zhao, H. J.; Momand, J.; Everhardt, A. S.; Agnus, G.; Blake, G. R.; Lecoœur, P.; Kooi, B. J.; Íñiguez, J.; Dkhil, B.;

- Noheda, B. A Rhombohedral Ferroelectric Phase in Epitaxially Strained  $\text{Hf}_{0.5}\text{Zr}_{0.5}\text{O}_2$  Thin Films. *Nat. Mater.* **2018**,
- (18) Robertson, J. High Dielectric Constant Gate Oxides for Metal Oxide Si Transistors. *Rep. Prog. Phys.* **2005**, *69*, 327–396.
- (19) Starschich, S.; Boettger, U. An Extensive Study of the Influence of Dopants on the Ferroelectric Properties of  $\text{HfO}_2$ . *J. Mater. Chem. C* **2017**, *5*, 333–338.
- (20) Polakowski, P.; Müller, J. Ferroelectricity in Undoped Hafnium Oxide. *Appl. Phys. Lett.* **2015**, *106*, 232905.
- (21) Huan, T. D.; Sharma, V.; Rossetti, G. A.; Ramprasad, R. Pathways Towards Ferroelectricity in Hafnia. *Phys. Rev. B* **2014**, *90*, 064111.
- (22) Reyes-Lillo, S. E.; Garrity, K. F.; Rabe, K. M. Antiferroelectricity in Thin-Film  $\text{ZrO}_2$  from First Principles. *Phys. Rev. B* **2014**, *90*, 140103.
- (23) Sang, X.; Grimley, E. D.; Schenk, T.; Schroeder, U.; LeBeau, J. M. On the Structural Origins of Ferroelectricity in  $\text{HfO}_2$  Thin Films. *Appl. Phys. Lett.* **2015**, *106*, 162905.
- (24) Materlik, R.; Künneth, C.; Kersch, A. The Origin of Ferroelectricity in  $\text{Hf}_{1-x}\text{Zr}_x\text{O}_2$ : A Computational Investigation and a Surface Energy Model. *J. Appl. Phys.* **2015**, *117*, 134109.
- (25) Batra, R.; Tran, H. D.; Ramprasad, R. Stabilization of Metastable Phases in Hafnia Owing to Surface Energy Effects. *Appl. Phys. Lett.* **2016**, *108*, 172902.
- (26) Künneth, C.; Materlik, R.; Kersch, A. Modeling Ferroelectric Film Properties and Size Effects from Tetragonal Interlayer in  $\text{Hf}_{1-x}\text{Zr}_x\text{O}_2$  Grains. *J. Appl. Phys.* **2017**, *121*, 205304.
- (27) Park, M. H.; Lee, Y. H.; Kim, H. J.; Schenk, T.; Lee, W.; Kim, K. D.; Fengler, F. P. G.; Mikolajick, T.; Schroeder, U.; Hwang, C. S. Surface and Grain Boundary Energy as the

Key Enabler of Ferroelectricity in Nanoscale Hafnia-Zirconia: A Comparison of Model and Experiment. *Nanoscale* **2017**, *9*, 9973–9986.

- (28) Shiraishi, T.; Katayama, K.; Yokouchi, T.; Shimizu, T.; Oikawa, T.; Sakata, O.; Uchida, H.; Imai, Y.; Kiguchi, T.; Konno, T. J.; Funakubo, H. Impact of Mechanical Stress on Ferroelectricity in  $(\text{Hf}_{0.5}\text{Zr}_{0.5})\text{O}_2$  Thin Films. *Appl. Phys. Lett.* **2016**, *108*, 262904.
- (29) Batra, R.; Huan, T. D.; Jones, J. L.; Rossetti, G.; Ramprasad, R. Factors Favoring Ferroelectricity in Hafnia: A First-Principles Computational Study. *J. Phys. Chem. C* **2017**, *121*, 4139–4145.
- (30) Park, M. H.; Schenk, T.; Fancher, C. M.; Grimley, E. D.; Zhou, C.; Richter, C.; LeBeau, J. M.; Jones, J. L.; Mikolajick, T.; Schroeder, U. A Comprehensive Study on the Structural Evolution of  $\text{HfO}_2$  Thin Films Doped with Various Dopants. *J. Mater. Chem. C* **2017**, *5*, 4677–4690.
- (31) Xu, L.; Nishimura, T.; Shibayama, S.; Yajima, T.; Migita, S.; Toriumi, A. Kinetic Pathway of the Ferroelectric Phase Formation in Doped  $\text{HfO}_2$  Films. *J. Appl. Phys.* **2017**, *122*, 124104.
- (32) Batra, R.; Huan, T. D.; Rossetti, G. A.; Ramprasad, R. Dopants Promoting Ferroelectricity in Hafnia: Insights from a comprehensive Chemical Space Exploration. *Chem. Mater.* **2017**, *29*, 9102–9109.
- (33) Xu, L.; Nishimura, T.; Shibayama, S.; Yajima, T.; Migita, S.; Toriumi, A. Ferroelectric Phase Stabilization of  $\text{HfO}_2$  by Nitrogen Doping. *Appl. Phys. Express* **2016**, *9*, 091501.
- (34) Zhou, D.; Xu, J.; Li, Q.; Guan, Y.; Cao, F.; Dong, X.; Müller, J.; Schenk, T.; Schröder, U. Wake-up Effects in Si-Doped Hafnium Oxide Ferroelectric Thin Films. *Appl. Phys. Lett.* **2013**, *103*, 192904.

- (35) Schenk, T.; Yurchuk, E.; Mueller, S.; Schroeder, U.; Starschich, S.; Böttger, U.; Mikolajick, T. About the Deformation of Ferroelectric Hystereses. *Appl. Phys. Rev.* **2014**, *1*, 041103.
- (36) Lee, C.-K.; Cho, E.; Lee, H.-S.; Hwang, C. S.; Han, S. First-Principles Study on Doping and Phase Stability of HfO<sub>2</sub>. *Phys. Rev. B* **2008**, *78*, 012102.
- (37) Schlom, D. G.; Chen, L. Q.; Eom, C. B.; Rabe, K. M.; Streiffer, S. K.; Triscone, J. M. Strain Tuning of Ferroelectric Thin Films. *Ann. Rev. Mater. Res.* **2007**, *37*, 589–626.
- (38) Damodaran, A. R.; Agar, J. C.; Pandya, S.; Chen, Z.; Dedon, L.; Xu, R.; Apgar, B.; Saremi, S.; Martin, L. W. New Modalities of Strain-Control of Ferroelectric Thin Films. *J. Phys.: Condens. Matter* **2016**, *28*, 263001.
- (39) Angsten, T.; Martin, L. W.; Asta, M. Orientation-Dependent Properties of Epitaxially Strained Perovskite Oxide Thin Films: Insights from First-Principles Calculations. *Phys. Rev. B* **2017**, *95*, 174110.
- (40) Xu, R.; Karthik, J.; Damodaran, A. R.; Martin, L. W. Stationary Domain Wall Contribution to Enhanced Ferroelectric Susceptibility. *Nat. Comm.* **2014**, *5*, 3120.
- (41) Xu, R.; Liu, S.; Grinberg, I.; Karthik, J.; Damodaran, A. R.; Rappe, A. M.; Martin, L. W. Ferroelectric Polarization Reversal via Successive Ferroelastic Transitions. *Nat. Mater.* **2015**, *14*, 79–86.
- (42) Park, M. H.; Kim, H. J.; Kim, Y. J.; Moon, T.; Hwang, C. S. The Effects of Crystallographic Orientation and Strain of Thin Hf<sub>0.5</sub>Zr<sub>0.5</sub>O<sub>2</sub> Film on Its Ferroelectricity. *Appl. Phys. Lett.* **2014**, *104*, 072901.
- (43) Katayama, K.; Shimizu, T.; Sakata, O.; Shiraishi, T.; Nakamura, S.; Kiguchi, T.; Akama, A.; Konno, T. J.; Uchida, H.; Funakubo, H. Growth of (111)-Oriented Epitaxial

- and Textured Ferroelectric Y-Doped HfO<sub>2</sub> Films for Downscaled Devices. *Appl. Phys. Lett.* **2016**, *109*, 112901.
- (44) Qian, G.-R.; Dong, X.; Zhou, X.-F.; Tian, Y.; Oganov, A. R.; Wang, H.-T. Variable Cell Nudged Elastic Band Method for Studying Solid–Solid Structural Phase Transitions. *Comput. Phys. Commun.* **2013**, *184*, 2111–2118.
- (45) Oganov, A. R.; Glass, C. W. Crystal Structure Prediction Using Ab Initio Evolutionary Techniques: Principles and Applications. *J. Chem. Phys.* **2006**, *124*, 244704.
- (46) Lyakhov, A. O.; Oganov, A. R.; Stokes, H. T.; Zhu, Q. New Developments in Evolutionary Structure Prediction Algorithm USPEX. *Comput. Phys. Commun.* **2013**, *184*, 1172–1182.
- (47) Oganov, A. R.; Lyakhov, A. O.; Valle, M. How Evolutionary Crystal Structure Prediction Works—and Why. *Acc. Chem. Res.* **2011**, *44*, 227–237.
- (48) Giannozzi, P. et al. Quantum ESPRESSO: A Modular and Open-Source Software Project for Quantum Simulations of Materials. *J. Phys.: Condens. Matter* **2009**, *21*, 395502.
- (49) Garrity, K. F.; Bennett, J. W.; Rabe, K. M.; Vanderbilt, D. Pseudopotentials for High-Throughput DFT Calculations. *Comput. Mater. Sci.* **2014**, *81*, 446–452.
- (50) Henkelman, G.; Uberuaga, B. P.; Jónsson, H. A Climbing Image Nudged Elastic Band Method for Finding Saddle Points and Minimum Energy Paths. *J. Chem. Phys.* **2000**, *113*, 9901–9904.
- (51) Park, M. H.; Lee, Y. H.; Kim, H. J.; Kim, Y. J.; Moon, T.; Kim, K. D.; Hyun, S. D.; Mikolajick, T.; Schroeder, U.; Hwang, C. S. Understanding the Formation of the Metastable Ferroelectric Phase in Hafnia–Zirconia Solid Solution Thin Films. *Nanoscale* **2018**, *10*, 716–725.

- (52) Perdew, J. P.; Burke, K.; Ernzerhof, M. Generalized Gradient Approximation Made Simple. *Phys. Rev. Lett.* **1996**, *77*, 3865–3868.
- (53) Perdew, J. P.; Burke, K.; Ernzerhof, M. Generalized Gradient Approximation Made Simple [Phys. Rev. Lett. 77, 3865 (1996)]. *Phys. Rev. Lett.* **1997**, *78*, 1396–1396.

Table 1: Transition barriers between HfO<sub>2</sub> polymorphs. Energy in eV/f.u.

Phase Transition	Forward	Reverse
T → OA	0.067	0.162
T → PO	0.032	0.108
T → M	0.013	0.141
OA → PO	0.171	0.151
PO → M	0.109	0.162

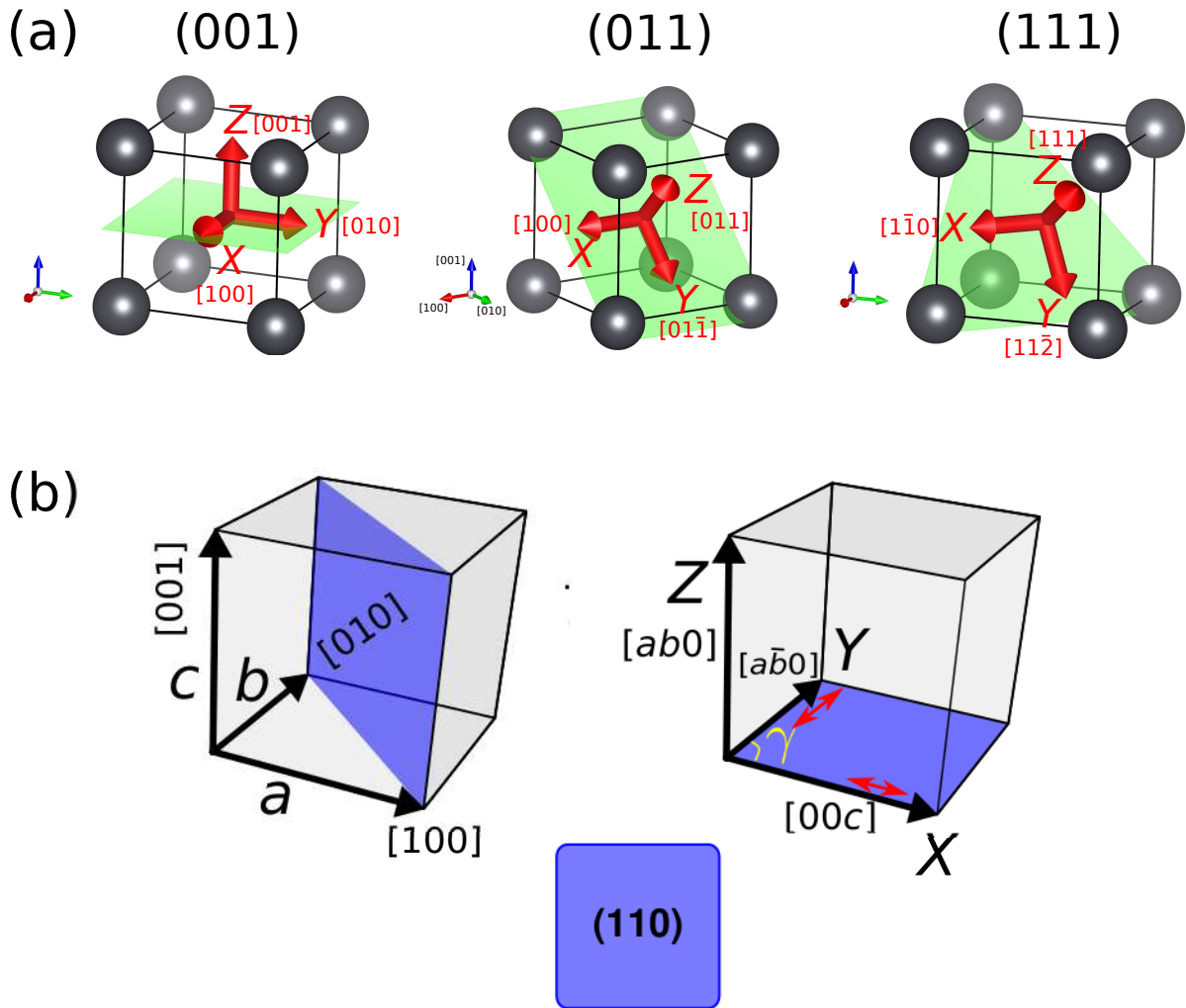


Figure 1: (a) Schematics of measurement axes for the (100)-, (110)-, and (111)-growth orientations for a cubic structure. (b) Illustration of the (110) orientation denoted as  $X[00c]Y[a\bar{b}0]Z[ab0]$  for a non-cubic structure. The  $XY$  plane is the epitaxial plane where the lattice vectors are scaled when applying the biaxial deformations while the  $Z$  axis is chosen as the surface normal direction that is free to relax.

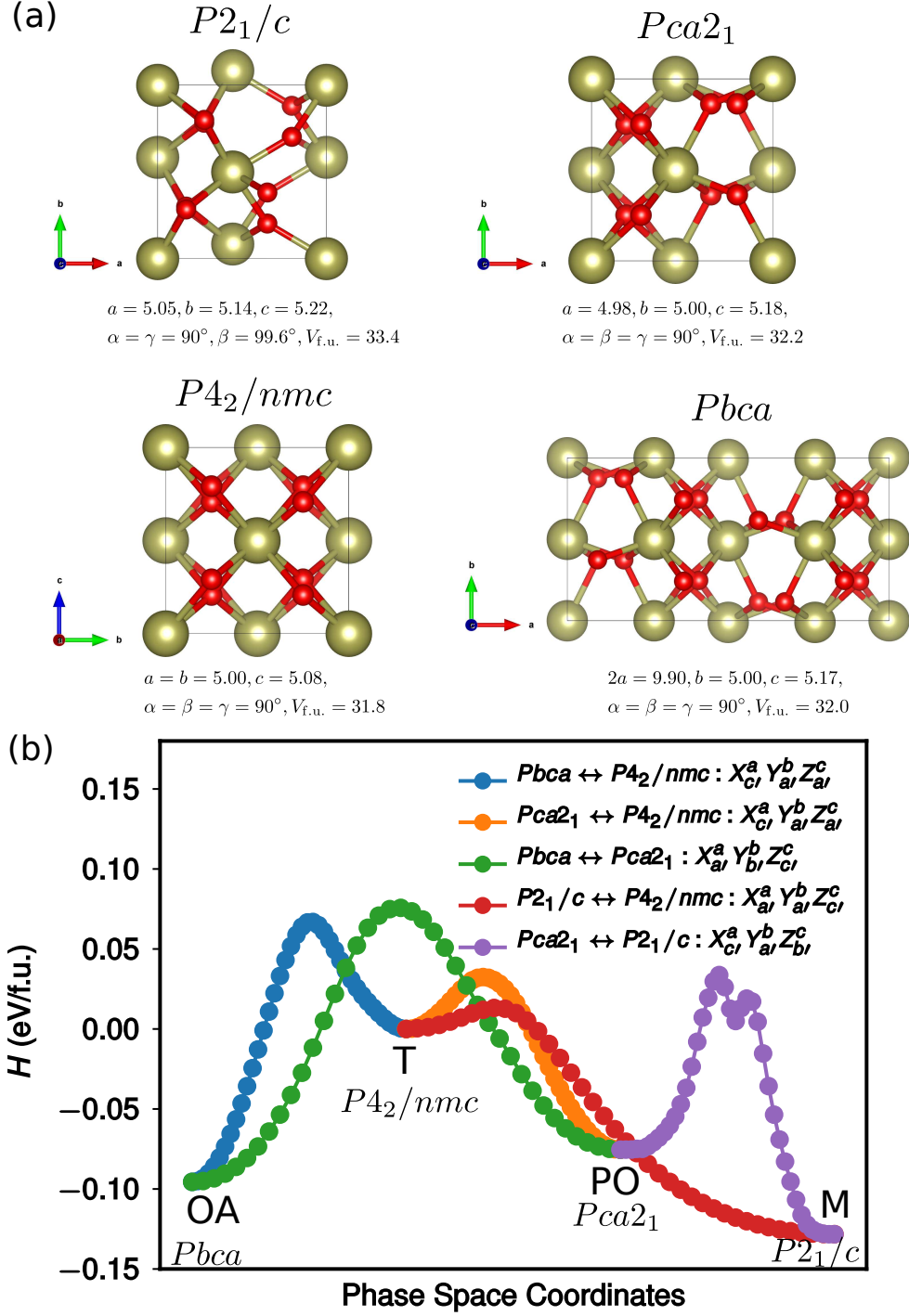


Figure 2: (a) Optimized lattice parameters of the  $P2_1/c$  (M),  $Pca2_1$  (PO),  $P4_2/nmc$  (T), and  $Pbca$  (OA) phases of  $HfO_2$ . Lattice constants in the unit of  $\text{\AA}$  and volume in the unit of  $\text{\AA}^3$ . (b) Minimum energy paths connecting different phases of  $HfO_2$  obtained with VC-NEB.

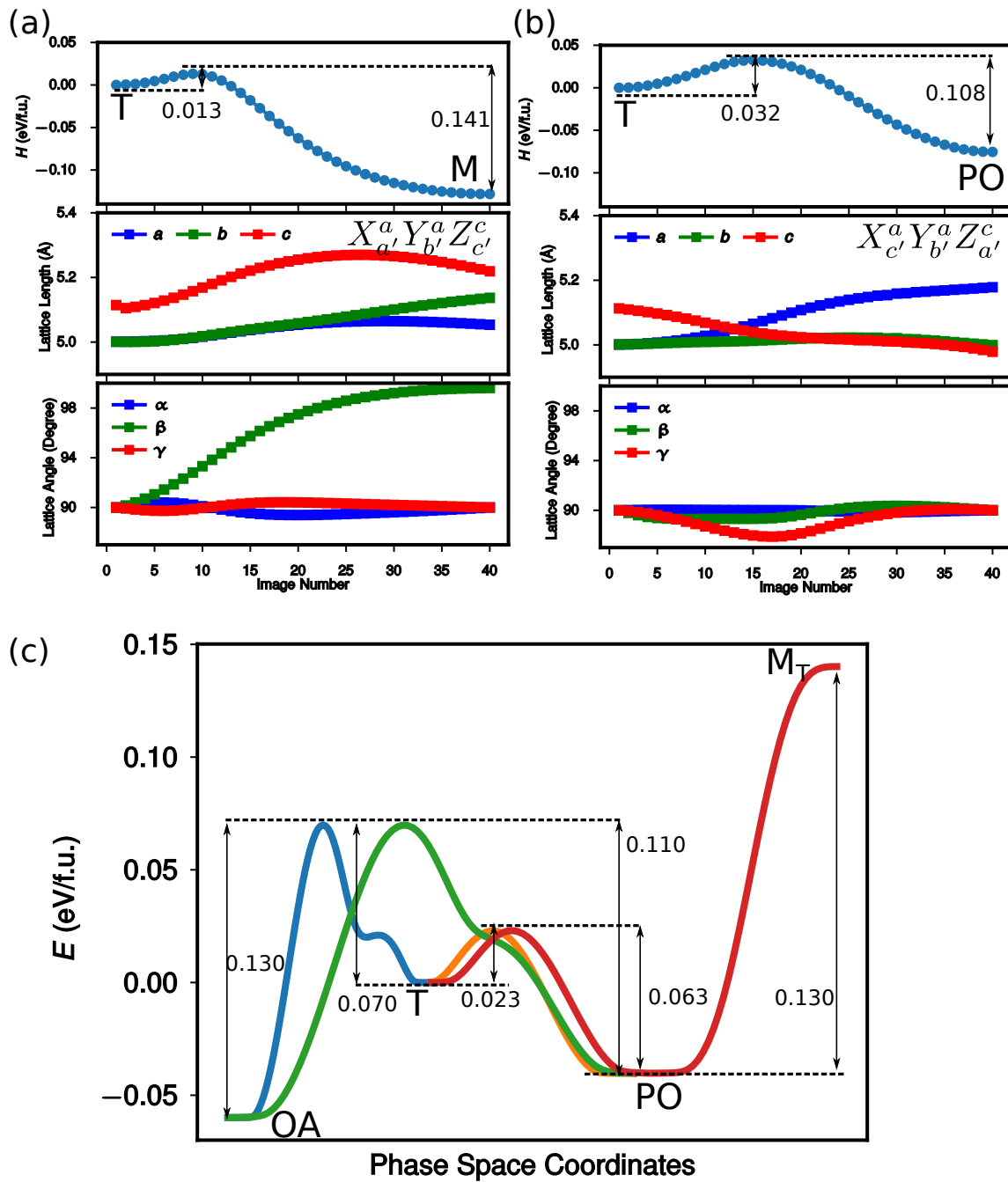


Figure 3: Enthalpy barrier and evolution of internal structural parameters for the (a) T → M and (b) T → PO phase transitions. (c) Phase transition paths obtained with NEB by fixing lattice constants to the values of the T phase.

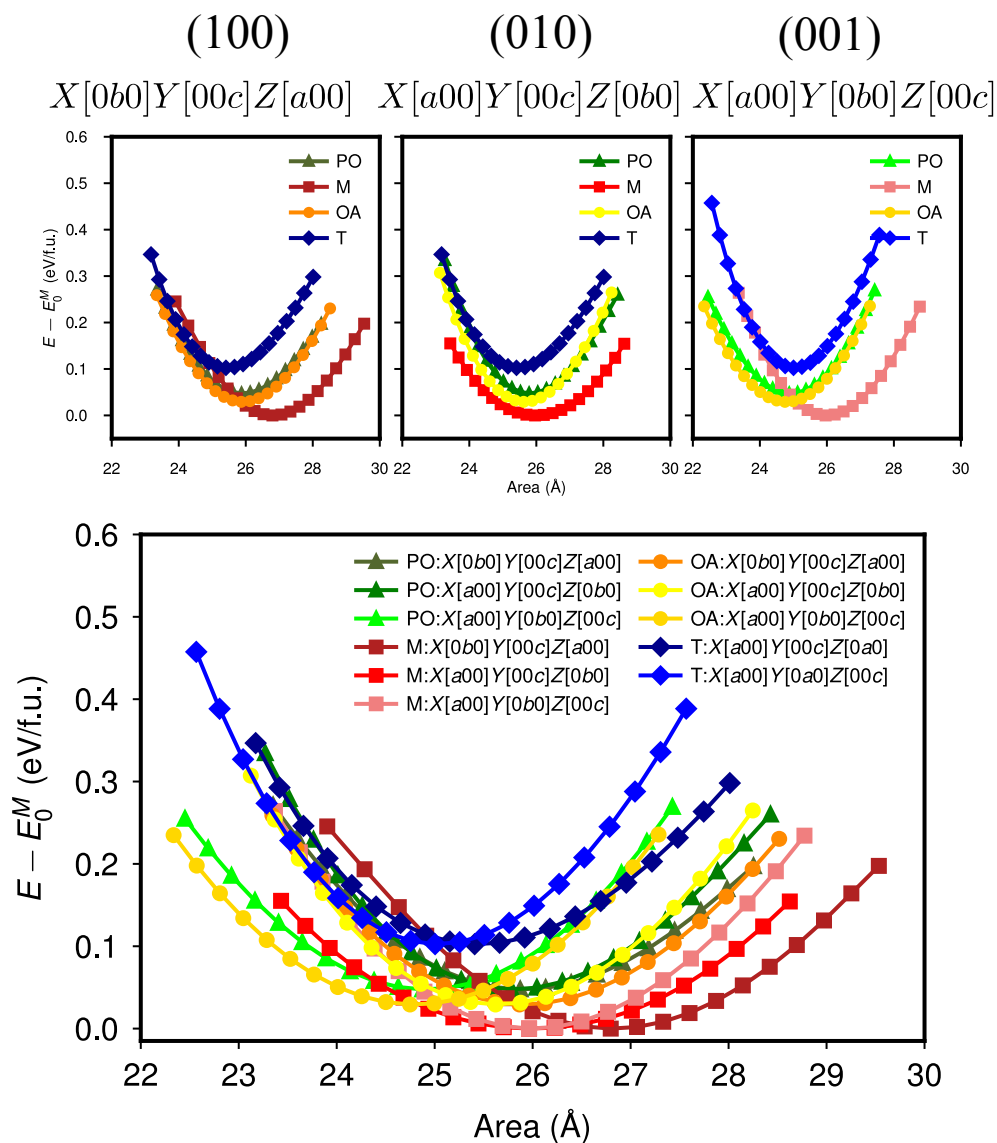


Figure 4: Energies of polymorphs of  $\text{HfO}_2$  in response to equibiaxial deformations applied in  $\{001\}$  planes. The energy of the equilibrium bulk M phase ( $E_M^0$ ) is chosen as the reference.

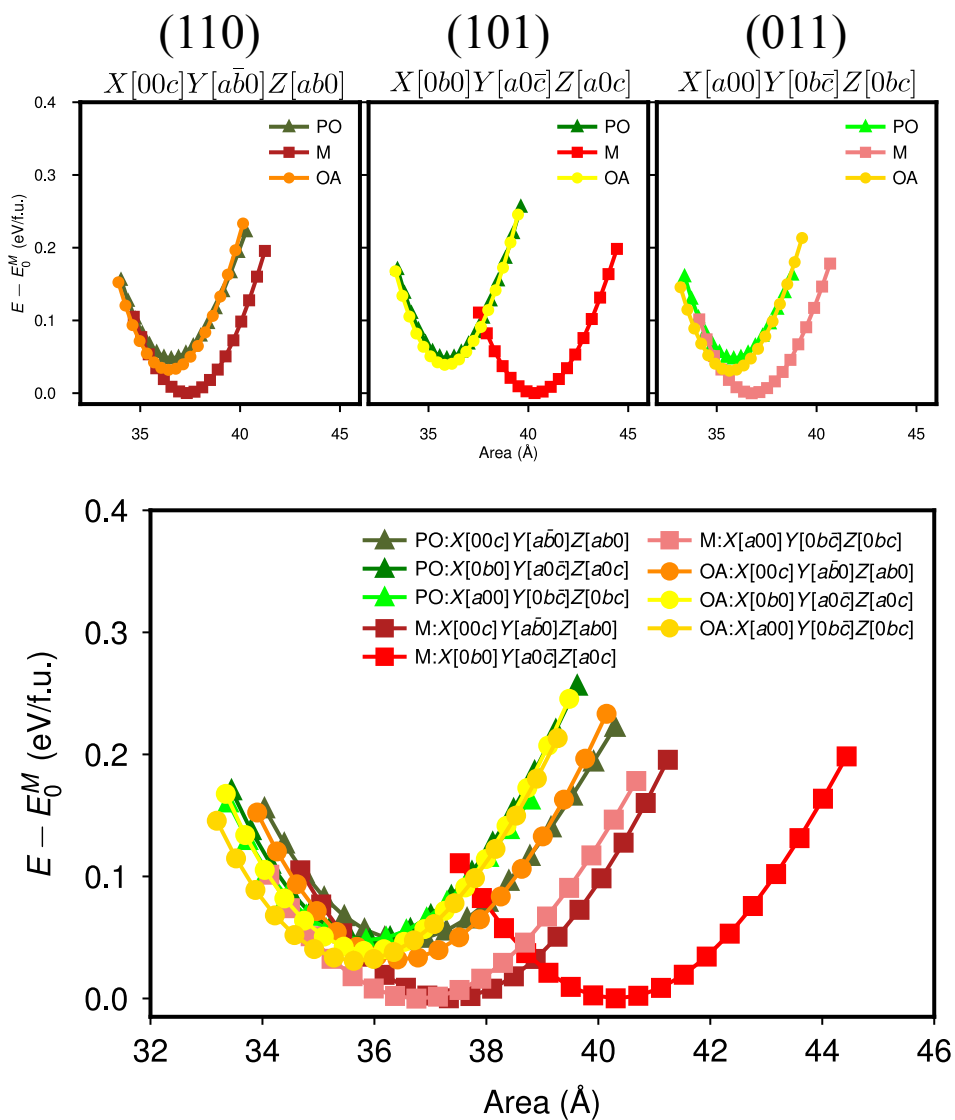


Figure 5: Energies of polymorphs of  $\text{HfO}_2$  in response to equibiaxial deformations applied in  $\{011\}$  planes.

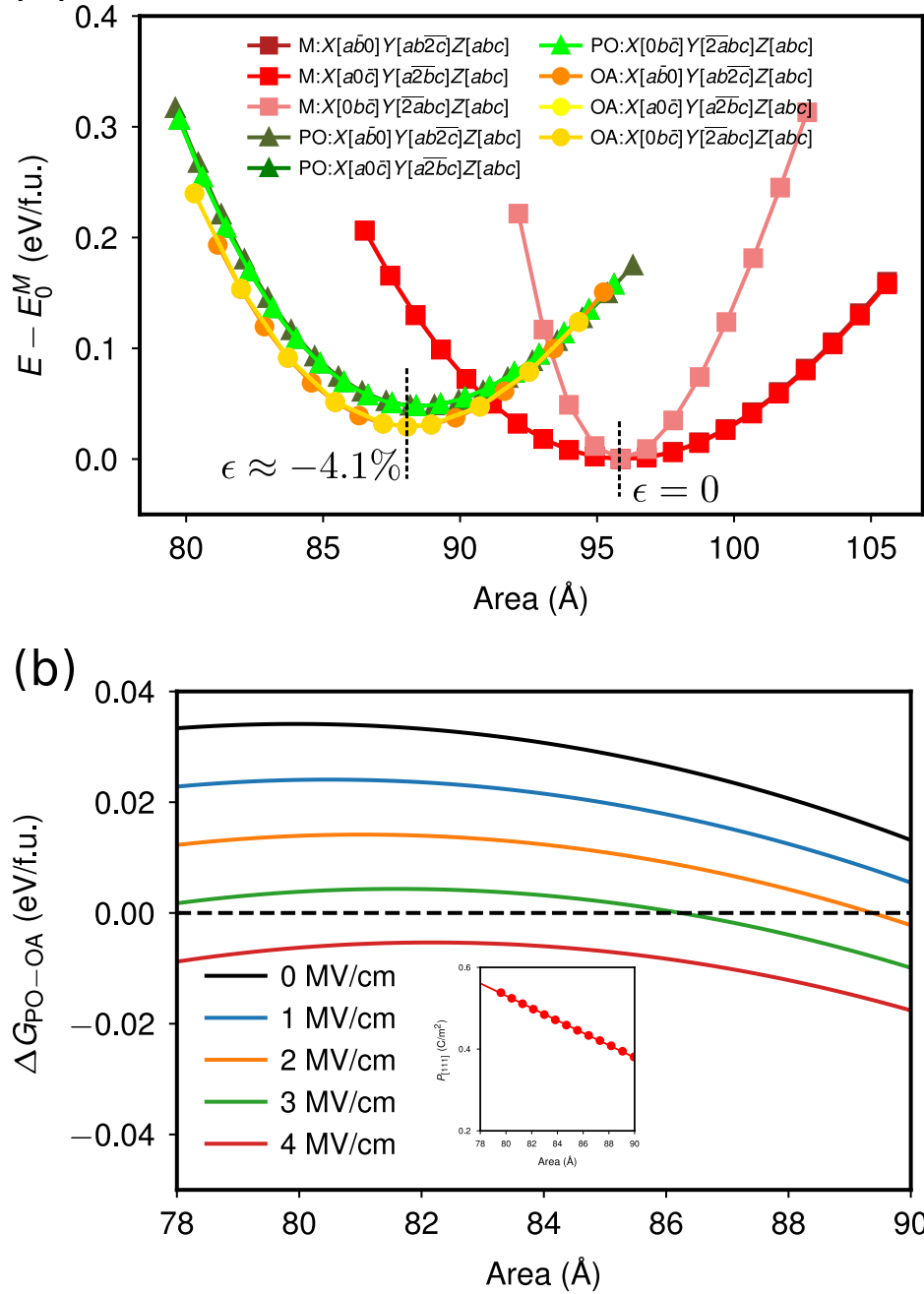


Figure 6: (a) Energies of polymorphs of  $\text{HfO}_2$  in response to equibiaxial deformations applied in  $\{111\}$  planes. (b) Effects of  $[111]$  electric fields on the free energy difference between PO and OA phases. The inset shows the polarization along the  $[111]$  direction ( $P_{111}$ ) as a function of in-plane misfit strains in the absence of electric fields.